Hindawi
Shock and Vibration
Volume 2019, Article ID 8729620, 20 pages
https://doi.org/10.1155/2019/8729620

Research Article

Extraction of Features due to Breathing Crack from Vibration Response of Rotated Blades considering Tenon Connection and Shroud Contact

Faming Yang, Yongmin Yang, Haifeng Hu, Fengjiao Guan, Guoji Shen, Suiyu Chen, and Zifang Bian

Science and Technology on Integrated Logistics Support Laboratory, National University of Defense Technology, Changsha 410072, China

Correspondence should be addressed to Yongmin Yang; yangyongmin@163.com

Received 15 April 2019; Revised 12 June 2019; Accepted 14 July 2019; Published 29 July 2019

Academic Editor: Zhixiong Li

Cracks are common failures of aeroengine rotated blades. Online monitoring of rotated blades through their vibration to identify cracks early in various working conditions is significant for operational safety. Breathing crack is a practical form of early cracks and results in nonlinear vibration response. Tenon connection and shroud contact are common structures in aeroengine rotated blades, which can also lead blades to vibrate nonlinearly and seriously interfere online identification of early cracks. Thus, it is important to extract vibration features due to breathing crack considering these two structures. Firstly, a blade with tenon and shroud is simplified and a lumped parameter model of the bladed disk is built. Then, dry friction and coupling force on a blade are analyzed and dynamics equations of the lumped parameter model are established. Next, the stiffness of the blade trunk with a breathing crack is analyzed. Finally, the vibration response of blade trunks with the occurrence of breathing crack is analyzed in time and frequency domains by numerical simulation. Effective features due to breathing crack for online identification are extracted. 2x components of spectrums can be the criterion to judge whether breathing crack occurs. Besides, by comparing the changes in vibration amplitudes with 1x component peaks of spectrums, the cracked blade trunk can be distinguished. These findings can provide important theoretical guidance for online identification of early cracks in aeroengine rotated blades.

1. Introduction

Aeroengine is a power source and a core component of aviation equipment. As one of the most fatigue and essential parts in aeroengine, rotated blades are important components for energy conversion. They suffer various loads including centrifugal force, airflow impact, and alternating forces transferred from other parts of the engine. Under these excitations, vibration happens and causes various faults in some fragile structures. As a common fault, crack is a key object of aeroengine blades monitoring. Once a crack occurs without detection, it may expand rapidly under complex forces and seriously affect the operational performance of the aeroengine, which may cause disasters. On the other hand, the occurrence of cracks can be reflected by changes in vibration characteristics. Thus, online monitoring of rotated blades through their vibration can be useful for cracks identification and significant for operational safety of aeroengines [1–3]. Effects of cracks on vibration characteristics of blades can be reflected by natural frequency, mode shape, vibration response, and so on. In fact, rotating speed of aeroengine blades is often changed. Even being controlled constant, rotating speed fluctuates due to various factors, such as uneven loads, airflow waves, and rotor imbalance [4, 5]. So it is difficult to measure the changes in natural frequency or mode shape online. But effects of cracks on vibration response of blades can be an important point for online identification. For assembled bladed disks, tenon connection and shroud contact are common structures. Blades are connected to mortises around disks by tenons and

transfer loads to disk. Besides, when blades vibrate, adjacent shrouds rub against each other. To some extent, these two structures can reduce vibration. But they also induce nonlinear characteristics, which have a great impact on vibration response of rotated blades in aeroengine [6–9]. This seriously interferes online identification of early cracks. Therefore, it is essential to extract features due to early crack from vibration response of rotated blades considering tenon connection and shroud contact.

Cracks can be generally divided into two types: open crack and breathing crack. Open crack is penetrating and remains open under various conditions. Nowadays, systematic research findings have been achieved about how open crack affects vibration characteristics of rotated blades and how to identify it online. Wu and Huang [10] made a research to study effects of an open crack on blades vibration characteristics considering various depths and locations under different rotating speeds. He et al. [11] proposed a new method to identify an open crack in turbine blades online under strong noise basing on genetic algorithm. However, early cracks are often nonpenetrating, and their contact surfaces can keep transforming with blades vibration. This kind of cracks can be modeled as breathing crack. Gudmundson [12] proved that damage on blades is oversimplified if open crack is used to model early cracks. However, periodic opening-closing behavior of breathing crack is more suitable to the real situation of early cracks.

Effects of breathing crack on blades vibration characteristics have attracted much attention in recent years. Various models have been built to simulate opening-closing behavior of breathing crack when blades are in working conditions, such as square wave function, cosine function, and some models that alter with loads changing [13–15]. Both open crack and breathing crack can change natural frequencies and mode shapes of blades. But breathing crack can cause nonlinear vibration response on blades. It is a big difference from open crack, which can be guidance for online identification of early cracks. Xu et al. [16] modeled breathing crack with a cosine function to analyze a single-blade vibration response. Then a method called vibration power flow analysis was utilized to catch subharmonics in vibration response of the blade caused by breathing crack. The finding provides a good criterion for early cracks online identification on a single blade with simple structure. However, blades are often not isolated. Tenon connection and shroud contact can bring coupling effects between blades. Since they can greatly change vibration characteristics of blades and even cause nonlinear vibration response, it is far from enough to detect breathing crack only with nonlinear characteristics. Considering tenon connection and shroud contact, online identification of early cracks can be a big challenge.

Tenon connection causes rotated blades to withstand nonlinear frictions. Laxalde and Thouverez [17] utilized nonlinear dry friction models on turbine blades and discussed the effects on blades vibration characteristics under different parameters. As nonlinear characteristics are induced, blades will present nonlinear vibration responses. Li et al. [18] established dry friction model for dovetail tenons and studied the effects on vibration response of blades under various rotating speeds, friction coefficients, and external force amplitudes. It is found that, in certain conditions, vibration responses of tenons include harmonics not only with the same frequency as excitation force but its 3x and 5x components. Apart from dry friction, coupling force between blades is also nonlinear due to inevitable gaps between tenons and mortises. Zeng et al. [19] analyzed dry friction and coupling force in consideration of gaps and established dynamic equations based on a lumped parameter model of mistuned bladed disk. Through a numerical simulation analysis, harmonics with multiple frequencies of excitation force were found in vibration response on tenons. Thus, it can be concluded that tenon connection causes nonlinear vibration response on blades.

Shroud contact is usually utilized to reduce vibration on blades in aeroengines. Dry friction between contact interfaces of adjacent shrouds can subtract vibration energy. On the other hand, it can cause nonlinear vibration response on blades. Yang et al. [20] proposed a contact friction model and delimit boundary conditions of three states: sticking, slipping, and separation. Besides, nonlinear dry friction is also modeled when two interfaces contact. Ji et al. [21] measured vibration response of blade trunks with damping and pointed out that nonlinear characteristics of vibration response are due to dry friction force. Voldřich et al. [22] studied nonlinear vibration response on blades induced by friction force between shrouds under sticking, slipping, and separation states, respectively. Wu et al. [23] characterized dry friction between shrouds with a nonlinear model to study the effects on blades vibration characteristics under various normal loads and external force. The study shows that shroud contact can lead rotated blades to vibrate nonlinearly.

To sum up, it can be concluded that tenon connection and shroud contact can both cause nonlinear vibration response on blades, which can seriously interfere online identification of early cracks. When these two structures exist, online identification of cracks based on vibration response of blades can be a big challenge. Thus, how breathing crack affects the vibration response of blades with tenon connection and shroud contact should be analyzed. And it is urgently needed to extract features which are effective for online identification due to breathing crack from vibration response. However, research on this area has rarely been reported so far.

Effects of breathing crack on vibration responses of blades are investigated by numerical simulation considering tenon connection and shroud contact. Based on it, features due to breathing crack are extracted to provide theoretical guidance for online identification. Contents of this paper are organized as follows: In Section 2, a real blade with tenon and shroud is simplified and a lumped parameter model of bladed disk is built. Then, nonlinear forces on blades are analyzed and dynamic equations of the lumped parameter model are established. In Section 3, a blade trunk is regarded as a cantilever beam. Stiffness model of the blade trunk containing a breathing crack is established. In Section 4, effects on the stiffness of blade trunk by a breathing crack are

further analyzed. Vibration responses of blades are obtained by solving the dynamic equations. Then, effects of breathing crack on vibration responses of blade trunks are analyzed in time and frequency domains. Based on it, features due to breathing crack effective for online identification are extracted. Finally, conclusions are drawn in Section 5.

2. Forced Vibration Modeling and Analysis of Blades considering Tenon Connection and Shroud Contact

2.1. Establishment of Lumped Parameter Model Based on a Bladed Disk. A blade can be divided into tenon and blade trunk. Tenon is connected with mortise on the outer edge of the disk. Forces on a blade are transferred to disk by tenon connection. When rotating at high speed in aeroengine, blade trunks inevitably vibrate under complex forces including airflow impacts. Excessive vibration can lead to failure and damage, which is harmful to operational safety of aeroengines. To reduce vibration, shrouds are often processed on blade trunks. It can extend life of blades as well as improve safety and stability of aeroengines. A type of blade with tenon and shroud is shown in Figure 1. It can be seen that geometry structure of a real blade is rather complicated. The blade trunk has pretwist angle and presetting angle. Even tenon and shroud have no regular shape.

Since tenon is subjected to dry friction and pressure by disk in rotating direction, simplify it to a cuboid, which withstands dry friction on its bottom surfaces and pressure on its side surfaces. The bevels of shroud are its contact interfaces. So consider shroud as a flat plate with a sharp angle. Affected by external forces and shroud contact, blade trunk will present bending and torsional vibration. But only bending vibration is studied here. Thus, blade trunk can be considered as a beam with shroud. The simplified model is shown in Figure 2.

Tenon connection and shroud contact can cause complex nonlinear forces on blades. Bottom surface of tenon is tightly attached to mortise and there exists a normal load. Disk drives blades to rotate by dry friction in the tangential direction between interfaces of tenon contact. Gaps are inevitable between side surfaces of tenon and mortise, so tenon may slip in mortise along their contact interfaces. In slipping state, the dry friction between tenon and mortise is relative to slipping direction. Besides, for disk is not an absolutely rigid body, it has a slight deformation under stress by a tenon and will impact adjacent ones. Therefore, coupling force exists between tenons. There is also dry friction force between adjacent shrouds, which is relative to the motion of their contact interfaces [8, 19, 24–26].

Three sectors are selected to build a lumped parameter model of a bladed disk similar to that in [19], as shown in Figure 3. In this model, the disk is considered as a flexible body with no mass. Equivalent mass of each tenon and blade trunk is m_i and m_{i+n}, respectively, where $i = 1, 2, \ldots, n$, and n is the total number of blades. What need to be declared is that shroud is included in the blade trunk by default. Equivalent stiffness of tenon and blade trunk is k_i and k_{i+n},

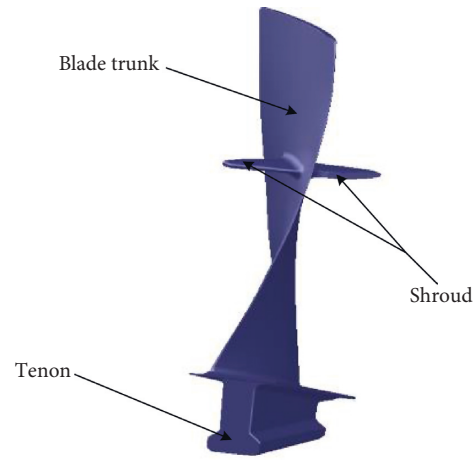

Figure 1: A certain type of blade with tenon and shroud.

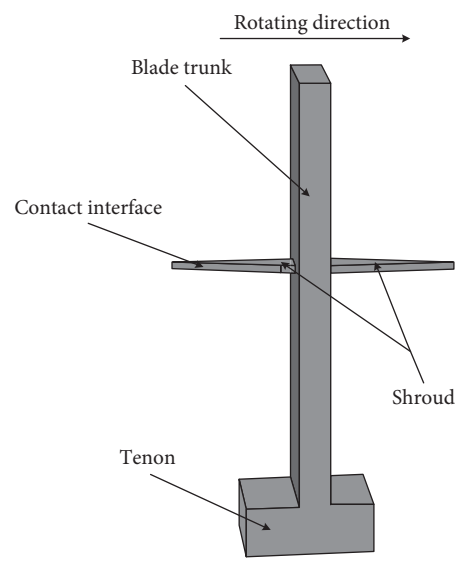

Figure 2: A simplified model of blade with tenon and shroud.

respectively. Equivalent damping of tenon and blade trunk is c_i and c_{i+n}, respectively. Taking the disk as a reference system, displacements of tenon and blade trunk are x_i and x_{i+n}, respectively. fl_i and fr_i are the coupling forces on tenon, and g_i is the dry friction force on tenon. Fl_i and Fr_i are the dry friction forces on shroud. f_i is the external airflow force on blade trunk.

2.2. Analysis of Nonlinear Forces on Blades. Tenon connection and shroud contact can cause nonlinear forces on rotated blades under working condition, which are analyzed in this section to lay the groundwork for subsequent research on vibration response.

2.2.1. Analysis of Dry Friction Force and Coupling Forces on Tenon. Forces on tenons are shown in Figure 4. i^{th} sector is analyzed. dl_i is the initial gap size between mortise and the left side of tenon, while dr_i is the initial gap size between

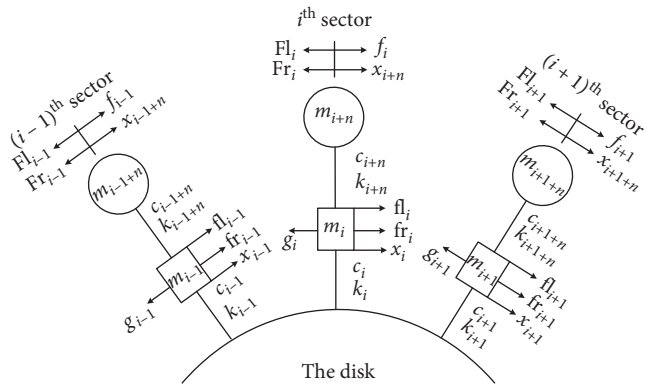

Figure 3: The lumped parameter model of a bladed disk.

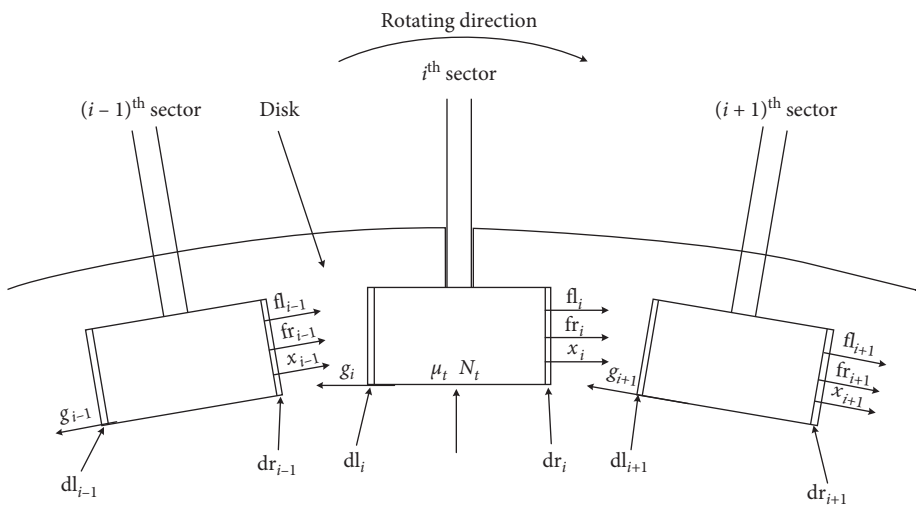

Figure 4: Diagram of forces on tenons.

mortise and the right side of tenon. A tenon withstands dry friction force g_i by the corresponding mortise and coupling forces fl_i and fr_i, respectively, by left and right adjacent ones.

Up till now, two types of model can be utilized to simulate contact friction performance: macroslip friction and microslip friction. Macroslip friction model only considers slipping states of interfaces [27], while microslip friction model considers both slipping states and sticking states [28]. Since vibration response of blade trunk is the main object to analyze in Section 4, and in sticking states, tenon has little effect on it, and macroslip friction model is used to simulate dry friction between tenon and mortise here. The friction coefficient of interfaces is expressed as μ_{t} and the normal load as N_{t}. Then, dry friction force g_i can be calculated as follows:

$$g_i = \mu_{\mathrm{t}} N_{\mathrm{t}} \mathrm{sgn}(\dot{x}_i). \tag{1}$$

In most studies about tenon connection, disks are considered as rigid bodies that cannot be deformed. In practice, disk has a slight deformation inevitably under loads by blades and affects other blades assembled on it, especially the adjacent ones. Coupling effects between adjacent blades by disk are essentially effects between their tenons. Coupling forces on adjacent tenons are related to gaps between their side surfaces and mortises. Firstly, coupling force on a tenon by its left adjacent one named fl_i is discussed. According to [8], when $(x_{i-1} - x_i) - (\mathrm{dr}_{i-1} + \mathrm{dl}_i) > 0$, the gaps between side surfaces of these two tenons and mortises are considered to be closed. At this time, coupling force is relatively larger and can be simulated as a linear elastic force. The coupling stiffness is set to be k_{g}. To simplify expression, $l_i = (x_{i-1} - x_i) - (\mathrm{dr}_{i-1} + \mathrm{dl}_i)$ is introduced. Then $\mathrm{fl}_i = k_{\mathrm{g}} l_i$. While $l_i \le 0$, the gaps between these two tenons and mortises are not closed. For the disk with a high stiffness, the coupling force is very small and can be neglected. To sum up, fl_i can be calculated as follows:

$$\mathrm{fl}_i = \begin{cases} k_{\mathrm{g}} l_i, & l_i > 0, \\ 0, & l_i \le 0. \end{cases} \tag{2}$$

In the same way, define $r_i = (x_i - x_{i+1}) - (\mathrm{dr}_i + \mathrm{dl}_{i+1})$. Coupling force on a tenon by its right adjacent one fr_i can be calculated as follows:

$$\mathrm{fr}_i = \begin{cases} -k_{\mathrm{g}} r_i, & r_i > 0, \\ 0, & r_i \le 0. \end{cases} \tag{3}$$

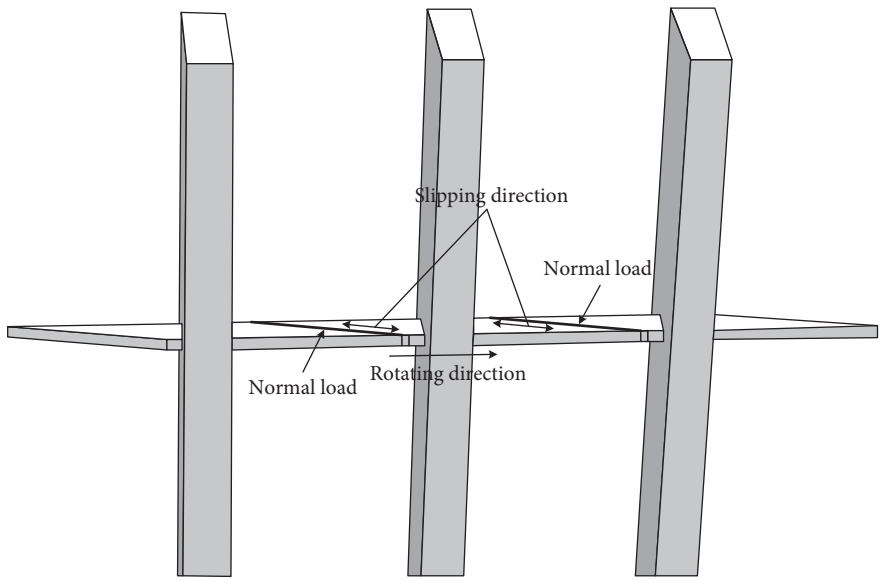

Figure 5: Diagram of shroud contact on a simplified blade.

2.2.2. Analysis of Dry Friction Forces on Shroud. When blades are assembled on a disk, their shrouds are attached and there exists normal loads between their interfaces. During rotation, excessive vibration on blades is avoided by dry friction between contact interfaces, as shown in Figure 5. In practice, directions of contact interfaces and rotation are at an angle. Therefore, directions of dry friction forces are not absolutely the same as that of rotation. But the stiffness of the blade trunk in rotating direction is much smaller than that in others, so the vibration is much larger. Furthermore, vibration in rotating direction is the main object of online monitoring. Considering these reasons, dry friction forces on shroud only in rotating direction are considered, or we can say that the component of actual dry friction force in rotating direction is considered.

Each shroud keeps in touch with its adjacent ones. The dry friction model proposed by Santhosh et al. [26] is applied, as shown in Figure 6. Contact of adjacent shrouds is regarded as a platform damper with a linear spring, whose stiffness is k_s. The friction coefficient is μ_s, and the normal load is N_s. yl_i and yr_i are displacements of left and right dampers, respectively. Dry friction forces Fl_i and Fr_i are relative to motion state of contact interfaces, which can be divided into two types: sticking and slipping. First, dry friction force by left adjacent shroud Fl_i is discussed. When $k_s|x_{i+n} - x_{i-1+n} - \mathrm{yl}_i| < \mu_s N_s$, the elastic force has not reached the lower limit of slipping friction. At this time, interfaces are in sticking state and Fl_i is equal to the elastic force. While $k_s|x_{i+n} - x_{i-1+n} - \mathrm{yl}_i| \geq \mu_s N_s$, elastic force has exceeded the lower limit of slipping friction. At this time, interfaces are in slipping state and Fl_i is equal to the slipping friction force. To sum up, Fl_i can be calculated as follows:

$$\mathrm{Fl}_i = \begin{cases} k_s\left(x_{i+n} - x_{i-1+n} - \mathrm{yl}_i\right), & k_s\left|x_{i+n} - x_{i-1+n} - \mathrm{yl}_i\right| < \mu_s N_s, \\ \mu_s N_s \operatorname{sgn}\left(\dot{\mathrm{yl}}_i\right), & k_s\left|x_{i+n} - x_{i-1+n} - \mathrm{yl}_i\right| \geq \mu_s N_s, \end{cases} \tag{4}$$

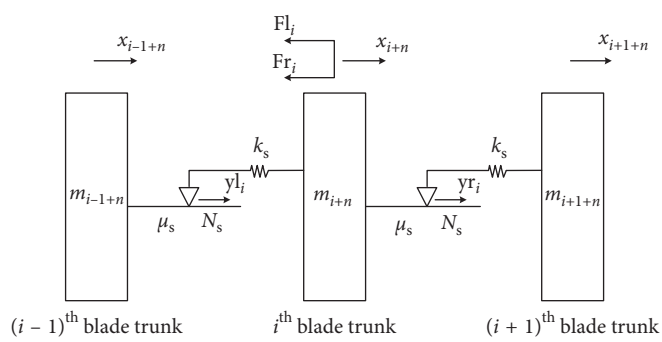

Figure 6: Dry friction model on shroud.

where damper's displacement yl_i and velocity $\dot{\mathrm{yl}}_i$ can be defined as follows:

$$\mathrm{yl}_i = \begin{cases} \left(x_{i+n} - x_{i-1+n}\right) - \left(\mu_s N_s / k_s\right), & \dot{x}_{i+n} - \dot{x}_{i-1+n} > 0, \\ 0, & \dot{x}_{i+n} - \dot{x}_{i-1+n} = 0, \\ \left(x_{i+n} - x_{i-1+n}\right) + \left(\mu_s N_s / k_s\right), & \dot{x}_{i+n} - \dot{x}_{i-1+n} < 0, \end{cases}$$
$$\dot{\mathrm{yl}}_i = \begin{cases} \dot{x}_{i+n} - \dot{x}_{i-1+n}, & \dot{x}_{i+n} - \dot{x}_{i-1+n} \neq 0, \\ 0, & \dot{x}_{i+n} - \dot{x}_{i-1+n} = 0. \end{cases} \tag{5}$$

Similar to Fl_i, dry friction force by right adjacent shroud Fr_i can be calculated as follows:

$$\mathrm{Fr}_i = \begin{cases} k_s\left(x_{i+n} - x_{i+1+n} - \mathrm{yr}_i\right), & k_s\left|x_{i+n} - x_{i+1+n} - \mathrm{yr}_i\right| < \mu_s N_s, \\ \mu_s N_s \operatorname{sgn}\left(\dot{\mathrm{yr}}_i\right), & k_s\left|x_{i+n} - x_{i+1+n} - \mathrm{yr}_i\right| \geq \mu_s N_s, \end{cases} \tag{6}$$

where damper's displacement yr_i and velocity $\dot{\mathrm{yr}}_i$ can be defined as follows:

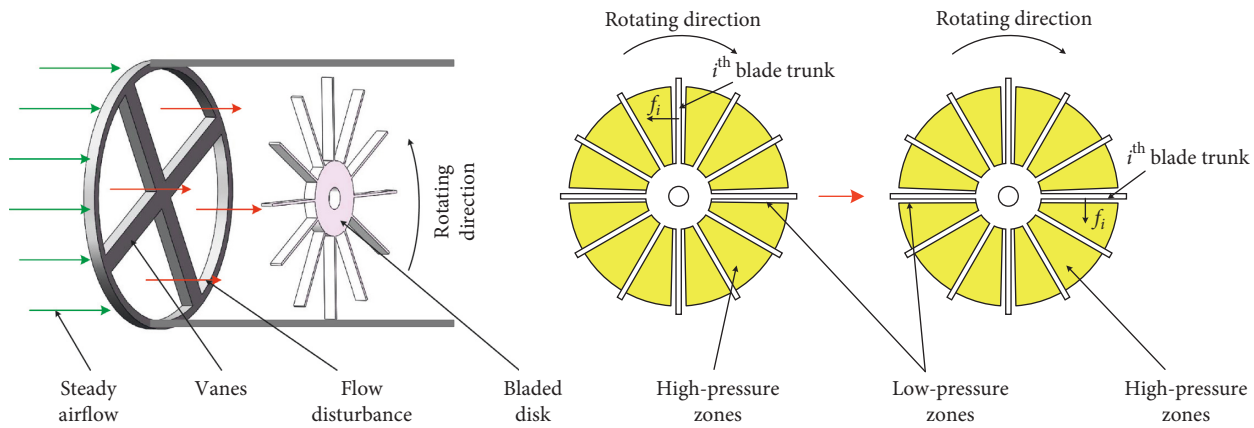

Figure 7: Diagram of airflow excitation.

$$\mathrm{yr}_i = \begin{cases} x_{i+n} - x_{i+1+n} - (\mu_s N_s/k_s), & \dot{x}_{i+n} - \dot{x}_{i+1+n} > 0, \\ 0, & \dot{x}_{i+n} - \dot{x}_{i+1+n} = 0, \\ x_{i+n} - x_{i+1+n} + (\mu_s N_s/k_s), & \dot{x}_{i+n} - \dot{x}_{i+1+n} < 0, \end{cases} \quad (7)$$

$$\dot{\mathrm{yr}}_i = \begin{cases} \dot{x}_{i+n} - \dot{x}_{i+1+n}, & \dot{x}_{i+n} - \dot{x}_{i+1+n} \neq 0, \\ 0, & \dot{x}_{i+n} - \dot{x}_{i+1+n} = 0. \end{cases}$$

2.3. Modeling of External Airflow Forces and Establishment of Dynamic Equations. In working conditions, blade trunks are subjected to airflow forces, as shown in Figure 7. Consider in one compressor stage, a set of vanes create an upstream flow disturbance with uneven air pressure around the bladed disk. Blade trunks circulate through high-pressure and low-pressure zones, and there exist external airflow forces. Take i^{th} blade trunk as an example. At the moment, it enters a high-pressure zone, and the airflow force is opposite to rotating direction because of pressure difference on both sides of blade trunk. In the same way, while it gets out from a high-pressure zone, the airflow force is the same as the rotating direction. Since blade trunks rotate at a rather high speed, it takes a very short time for them to pass through a pressure zone. Thus, airflow forces can be considered to be gradient forces. Similar to [29], airflow force f_i is simulated to a harmonic and cosine function which is utilized as follows:

$$f_i = f_0 \cos(\omega_{\text{excite}} t + \varphi_i), \quad (8)$$

where f_0 is the amplitude of force, ω_{excite} is the angular velocity of f_i, and $\omega_{\text{excite}} = 2\pi D E_0/60$. D is the rotating speed of the bladed disk, E_0 is the order of airflow force, which is equal to the number of transitions between high and low pressure in one circle around the bladed disk (also equal to the number of high-pressure zones or low-pressure zones), and φ_i is the phase angle and can be calculated as $\varphi_i = 2\pi E_0 (i-1)/n$.

According to the lumped parameter model shown in Figure 3 and force analysis on blades, dynamic equations of a simplified bladed disk can be established as equation (9). By solving it, the vibration response of blades under external airflow forces can be obtained:

$$\begin{cases} m_i \ddot{x}_i + c_i \dot{x}_i + c_{i+n}(\dot{x}_i - \dot{x}_{i+n}) + k_i x_i + k_{i+n}(x_i - x_{i+n}) = \mathrm{fl}_i + \mathrm{fr}_i - g_i, \\ m_{i+n} \ddot{x}_{i+n} + c_{i+n}(\dot{x}_{i+n} - \dot{x}_i) + k_{i+n}(x_{i+n} - x_i) = f_i - \mathrm{Fl}_i - \mathrm{Fr}_i. \end{cases} \quad (9)$$

3. Stiffness Modeling of Blade Trunk with a Breathing Crack

Since the tenon's stiffness is much larger than the blade trunk's and the movement range of tenon is rather small in practice, probability of cracks occurring in tenon is much lower than that in blade trunk. Thus, blade trunk with a breathing crack is focused, and the vibration responses of blade trunks are analyzed in the subsequent section.

Breathing crack affects vibration characteristics of the blade mainly by changing its bending stiffness rather than mass or damping. Therefore, the stiffness of the blade trunk with a breathing crack is focused.

Since shroud is thin and its proportion to blade trunk is low, its mass is relatively small and has little influence on bending stiffness of blade trunk, and it is omitted here. A blade trunk is simplified to a cantilever beam with one end fixed and one end free, as shown in Figure 8. The blade trunk's length is L, width is W, and thickness is H. There exists a breathing crack with a distance of y_c from the blade tip and the depth is d. First-order vibration is considered. According to [14], equivalent mass and stiffness of an intact blade trunk at statics state can be calculated as follows:

$$m_{i+n} = 0.228 m' L, \qquad k_p = \frac{EI\pi^4}{32L^3}. \quad (10)$$

where m' is the unit length mass of the blade trunk and can be calculated as $m' = \rho W H$, ρ is the material density of the blade trunk, E is Young's modulus, and I is the torque of the blade trunk around its central axis and can be calculated as $I = WH^3/12$.

According to [16], the blade trunk withstands the effects of centrifugal rigidity at high rotating speed, and its stiffness

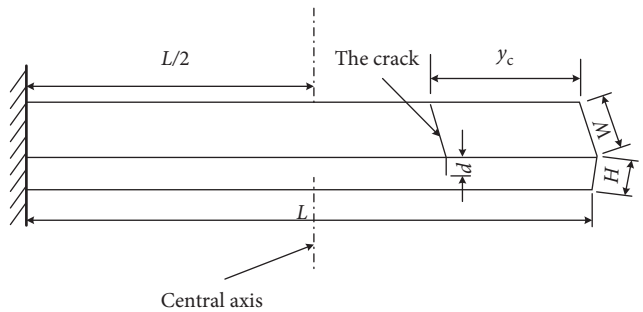

Figure 8: The simplified model of the blade trunk with a breathing crack.

is increased. Equivalent stiffness of the rotated blade trunk k_r can be calculated as follows:

$$k_r = k_p + 4\pi^2 m_{i+n} B n^2, \tag{11}$$

where B is the calibration factor and can be calculated as follows:

$$B = \left(\frac{\pi}{30}\right)^2 \frac{\int_0^L (R+y)\left[\int_0^Y (dz/dy)^2 dy\right] dy}{\int_0^L z^2 dy}, \tag{12}$$

where R is the radius of the disk and z is the modal function of a simplified blade trunk and can be calculated as follows:

$$z = (\sin\lambda_r y - \mathrm{sh}\lambda_r y) + \zeta_r(\cos\lambda_r - \mathrm{ch}\lambda_r y), \tag{13}$$

where $\zeta_r = (\cos\beta_r + \mathrm{ch}\beta_r)/(\sin\beta_r - \mathrm{sh}\beta_r)$ and $\lambda_r = \beta_r/L$. Since only the first-order mode is studied, $r = 1$ and $\beta_r = \beta_1 = 1.875$.

Consider a nonpenetrating crack occurs on the right side of ith blade trunk, as shown in Figure 9. In working conditions, it transits between two states: open and closed. At the moment entering a high-pressure zone, the blade trunk bends opposite to rotating direction under the airflow force. For tensile stress on that side, the breathing crack is open. At this time, the stiffness of the blade trunk is equal to that with an open crack. According to [16], crack brings additional flexibility to the blade trunk. Additional flexibility Δc can be calculated as follows:

$$\Delta c = \frac{72 y_c^2 \pi (1-\nu^2)}{EWH^4} g(\alpha), \tag{14}$$

where ν is Poisson's ratio and $g(\alpha)$ can be calculated as follows:

$$g(\alpha) = d^2\left(19.60\alpha^8 - 40.69\alpha^7 + 47.04\alpha^6 - 32.99\alpha^5 + 20.30\alpha^4 - 9.98\alpha^3 + 4.60\alpha^2 - 1.05\alpha^1 + 0.63\right), \tag{15}$$

where α is relative to the depth of the crack and thickness of the blade trunk and can be calculated as $\alpha = d/H$. Flexibility of an intact blade trunk can be calculated as $c_r = 1/k_r$. When breathing crack is fully open, the stiffness of the blade trunk can be calculated as follows:

$$k_{\text{ro}} = \frac{1}{\Delta c + c_r}. \tag{16}$$

While the blade trunk gets out of a high-pressure zone, it bends in the rotating direction under airflow force. The crack on it is closed under bearing stress, and stiffness of the blade trunk is equal to that when it is intact. Since breathing crack cyclically transits between open and closed states, stiffness of a rotated blade trunk is time-varying and coincides with transition of external airflow force. Thus, similar to [16], the stiffness of the blade trunk with a breathing crack can be simulated as follows:

$$k(t) = k_{\text{ro}} + \frac{1}{2}(k_r - k_{\text{ro}})(1 + \cos(\omega_{\text{excite}} t)). \tag{17}$$

Substitute $k(t)$ into equation (8) and solving it, the vibration response of the blade trunk with a breathing crack can be obtained.

4. Numerical Analysis of Effects by Breathing Crack on Vibration Response of Blade Trunks

Numerical analysis is done based on the dynamics model of the bladed disk in Section 2 and the stiffness model of blade trunk with a breathing crack in Section 3. Effects of breathing crack on vibration response are studied to extract features effective for online identification. Before the analysis, some parameters of the bladed disk have to be set, as shown in Table 1.

Due to minor differences in material, wear condition, and manufacturing, the physical property of each blade trunk cannot be exactly the same. According to [19], this phenomenon can be equivalent to stiffness mistuning. Stiffness mistuning factors are defined as $\delta_i = (k_{i+n} - k_r)/k_r$, and the stiffness of rotated blade trunks can be calculated as $k_{i+n} = k_r(1 + \delta_i)$. The stiffness mistuning factors are randomly generated satisfying the normal distribution with a mean of 0 and a standard deviation of 0.01. The factors corresponding to 12 blade trunks are shown in Table 2.

4.1. Effects on Stiffness of Blade Trunk by a Breathing Crack. It can be seen from the analysis in Section 3 that breathing crack changes stiffness of a blade trunk by introducing additional flexibility. Stiffness after a breathing crack occurs, and its relationship to related parameters is analyzed by numerical simulation.

As shown in Figure 10, the stiffness of a blade trunk with an open crack is less than that of an intact one, though they are constant. But once a breathing crack occurs, stiffness fluctuates between that of the above two cases. It reaches the level of intact trunk at a few moments, when it can be concluded that the crack is in a closed state. While it drops to the level with an open crack, fully open state is affirmed. In other cases, the crack is partly open. With stiffness decreasing, blade trunk can vibrate with larger amplitude after a breathing crack occurs. Furthermore, breathing crack can change the stiffness of blade trunk nonlinearly, which may affect frequencies in vibration response spectrum.

It is easy to find that the fluctuation range of stiffness depends on that with an open crack. And parameters y_c and

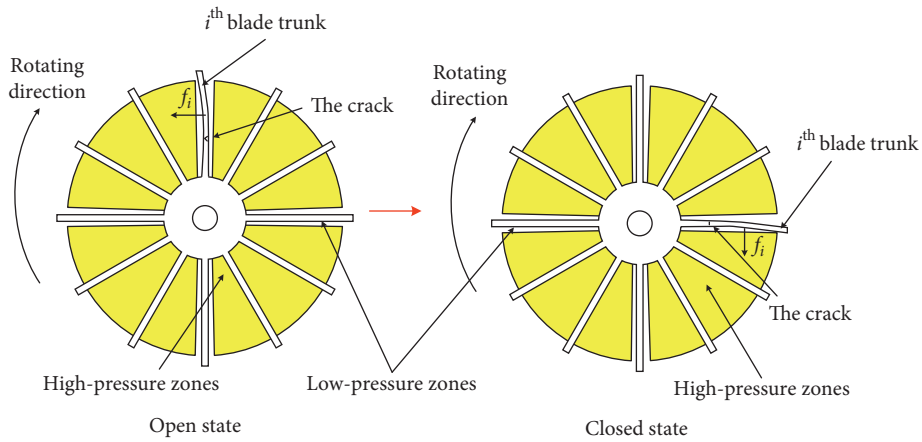

Figure 9: Diagram of breathing crack in open and closed states.

Table 1: Parameters of the bladed disk.

Symbols	Properties	Value
L	Length of a blade trunk (mm)	95
H	Thickness of a blade trunk (mm)	2.5
W	Width of a blade trunk (mm)	45
R	Radius of a disk (mm)	200
N	Total number of blades	12
E_0	Order of airflow force	1
D	Rotating speed (rpm)	5000
f_0	Amplitude of airflow force (N)	30
E	Young's modulus (Pa)	0.689×10^{11}
ν	Poisson's ratio	0.33
ρ	Material density of a blade trunk (kg/m^3)	2800
ξ	Damping ratio	0.01
m_t	Mass of a tenon (kg)	0.0272
c_t	Damping of a tenon (N·s/m)	0.1445
k_t	Stiffness of a tenon (N/m)	903480
k_g	Coupling stiffness of tenons (N/m)	361392
μ_t	Friction coefficient of tenon connection	0.5
N_t	Normal load on tenon bottom surface (N)	20
μ_s	Friction coefficient of shroud contact	0.5
N_s	Normal load on shroud contact interface (N)	10
k_s	Stiffness of shroud damping (N/m)	10000

d are related to it, according to equations (14) and (15). It means that location and depth are the factors affecting the stiffness of the blade trunk with an open crack. As shown in Figure 11, the stiffness of the blade trunk decreases with larger y_c and d, respectively, although the trends are nonlinear. Thus, it can be indicated that a breathing crack has a larger effect on vibration response of the blade trunk when it is deeper or closer to blade root.

Effects on vibration responses of blade trunks by breathing crack are analyzed in time and frequency domains in subsequent sections to extract features.

4.2. Extraction of Features in Time Domain. It is uniformly assumed that the breathing crack occurs in 1st blade trunk. As shown in Figure 12, the amplitude of the 1st blade trunk shows a steady upward trend with y_c and d, respectively, which is consistent with the analysis in Section 4.1. But for most other blade trunks, amplitudes fluctuate in various forms without obvious regularity and do not show much correlation with y_c and d. This indicates that tenon connection and shroud contact have effects on vibration responses. And these structures can bring great uncertainties to vibration amplitudes of blade trunks.

Next, comparison between vibration amplitudes of blade trunks is made. In order to provide a reference, vibration amplitudes of blade trunks with no crack occurring are shown in Figure 13. It can be seen that there are some differences and one of them is much higher than others. This phenomenon is called localization of vibration response, which is due to mistuning [30]. It is worth noting that the 1st blade trunk has a relatively medium amplitude.

Because of coupling effects between blades due to tenon connection and shroud contact, once breathing crack occurs in one blade trunk, vibration responses of others can be affected. Comparison between vibration amplitudes of blade trunks under different y_c and d is shown in Figure 14. It can be seen that localization of vibration response still exists after breathing crack occurs but is changed with y_c and d. The amplitude of the 1st blade trunk increases with y_c and d, respectively, and even becomes the largest with a distance of more than 65 mm or depth of more than 1.3 mm. However, location of vibration response is a phenomenon randomly existing between blades in different bladed disks. Thus, whether breathing crack occurs cannot be judged by comparison between amplitudes especially when the distance is short or the depth is shallow. But what can be noticed in Figure 14 is that the amplitude of the 1st blade trunk changes more rapidly than others. So it is worth focusing on the changes in vibration amplitudes after the occurrence of breathing crack.

A comparison between the changes in amplitudes of blade trunks after the occurrence of a breathing crack under different y_c and d is shown in Figure 15. The change equals amplitude of the blade trunk after crack minus that before crack. It can be seen that the changes in the amplitude of the 1st blade trunk is larger than others and the differences are obvious, under various y_c and d. From this feature, we can

Table 2: Stiffness mistuning factors of blade trunks.

δ_1	δ_2	δ_3	δ_4	δ_5	δ_6	δ_7	δ_8	δ_9	δ_{10}	δ_{11}	δ_{12}
0.0033	−0.0075	0.0137	−0.0171	−0.0010	−0.0024	0.0032	0.0031	−0.0086	−0.0003	−0.0016	0.0063

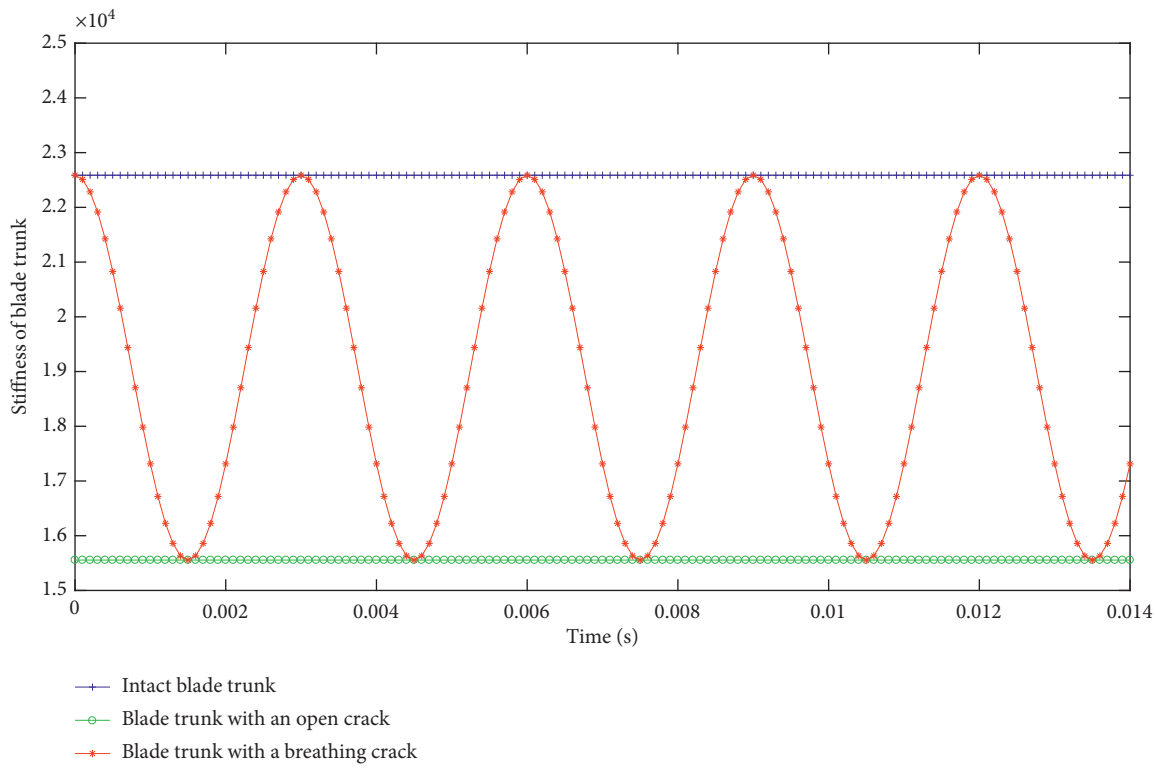

Figure 10: The stiffness graph of the blade trunk with time under different conditions.

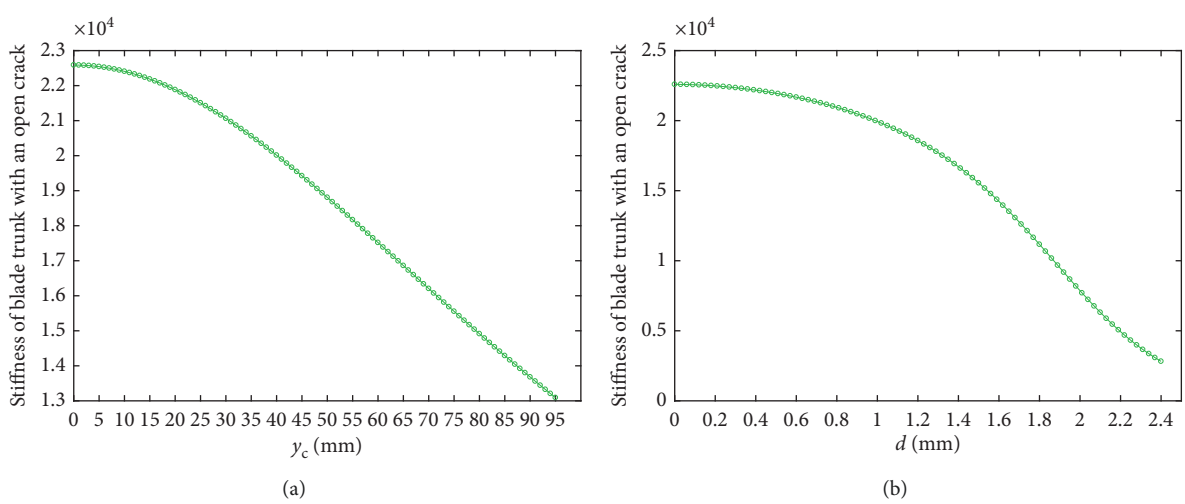

Figure 11: The stiffness graph of the blade trunk with (a) y_c and (b) d when there is an open crack. (a) The depth is set as $d = 1.5$ mm. (b) The distance is set as $y_c = 75$ mm.

know breathing crack occurs and distinguished the cracked blade trunk. Therefore, change in vibration amplitude can be a reliable evidence for online identification of breathing crack.

4.3. Extraction of Features in Frequency Domain. First, vibration response spectrum of each blade trunk without crack is obtained as a reference for subsequent analysis and shown in Figure 16. It can be seen that when no crack occurs, not

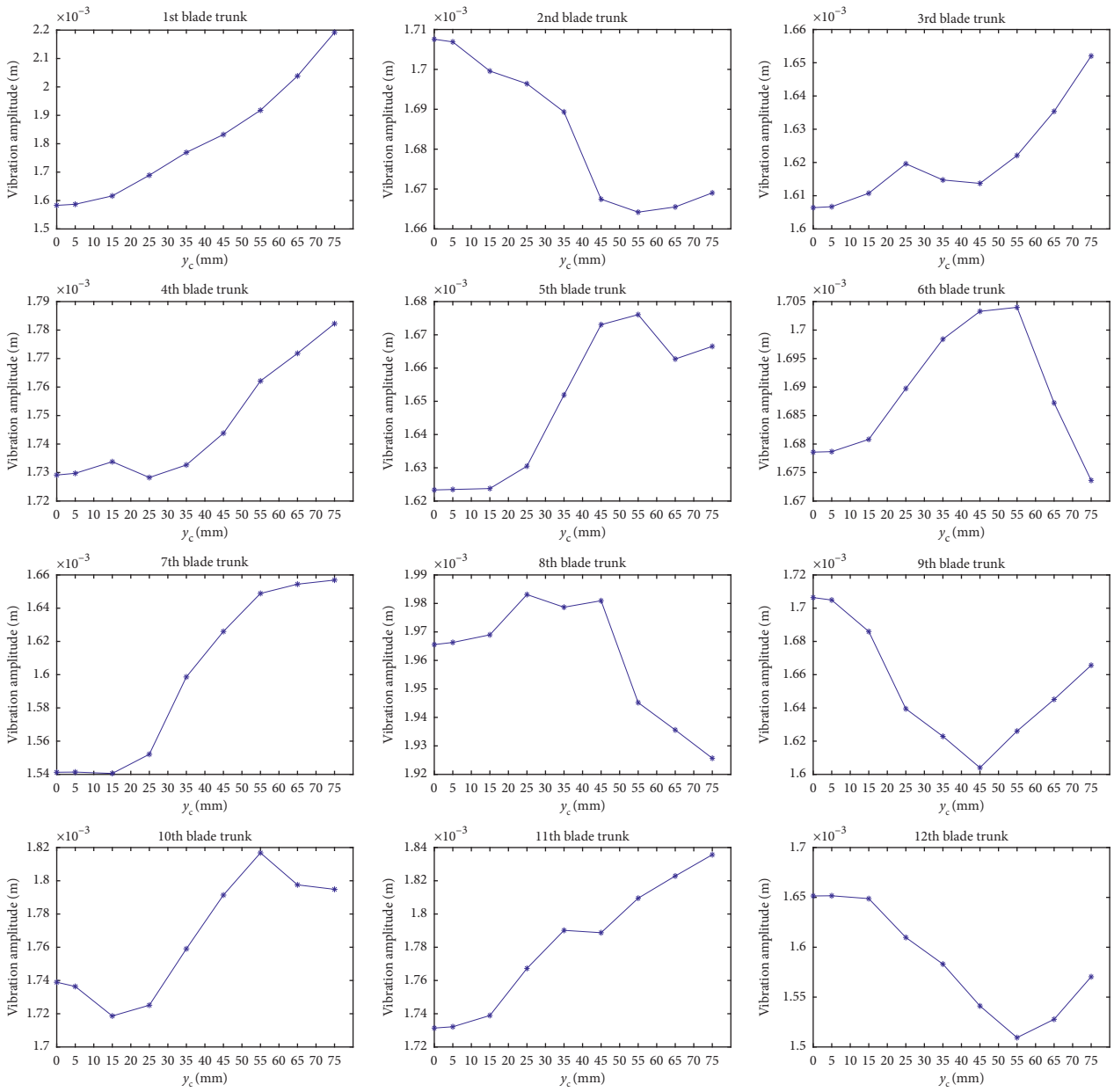

(a)

Figure 12: Continued.

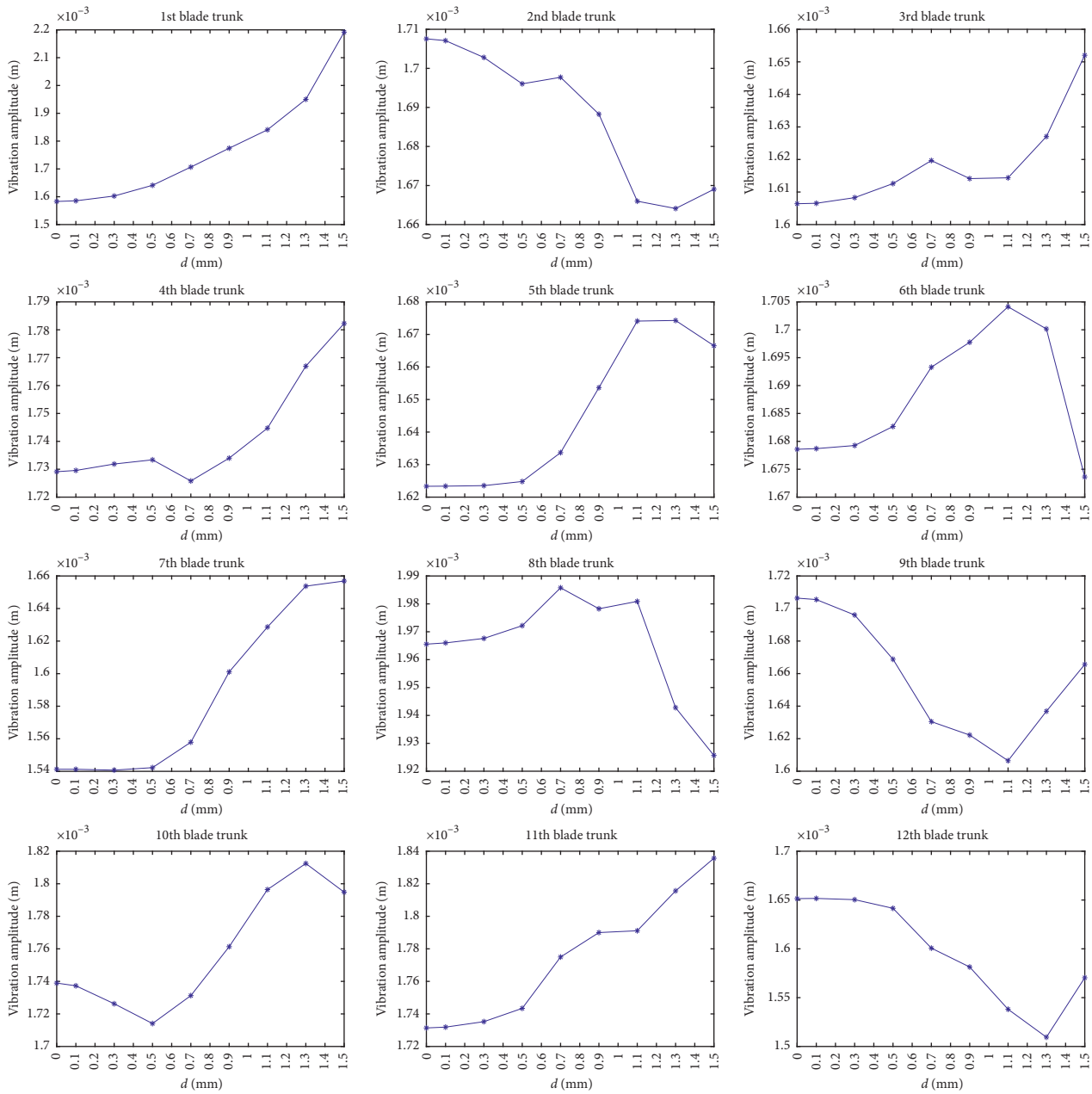

(b)

Figure 12: Vibration amplitude of each blade trunk with (a) the distance y_c and (b) the depth d. (a) The depth is set as $d = 1.5$ mm. (b) The distance is set as $y_c = 75$ mm.

only 1x but 3x and 5x components appear. This is a reflection of nonlinear characteristics, which is due to nonlinear forces induced by tenon connection and shroud contact.

Vibration response spectrum of each blade trunk after the occurrence of a breathing crack is shown in Figure 17. It can be seen that, in addition to 3x and 5x components, 2x and even 4x components appear in vibration response spectrum of each blade trunk. This proves that the appearance of breathing crack can lead to nonlinear vibration response. Thus, significant changes by breathing crack on vibration response of blade trunks can be found by frequency spectrum analysis. Since 2x components are more obvious than 4x components generally, choose them as features to judge that breathing crack occurs.

However, after a breathing crack occurs in the 1st blade trunk, 2x component appears not only in the vibration response spectrum of the 1st blade trunk, but that of all blade trunks. This is because coupling effects exist between blades due to tenon connection and shroud contact. Changes in vibration response of one blade can affect others. When we need to identify in which blade the breathing crack occurs, relying on 2x component is not enough. Then an attempt is made to extract features for determining the cracked blade trunk based on peaks in spectrums.

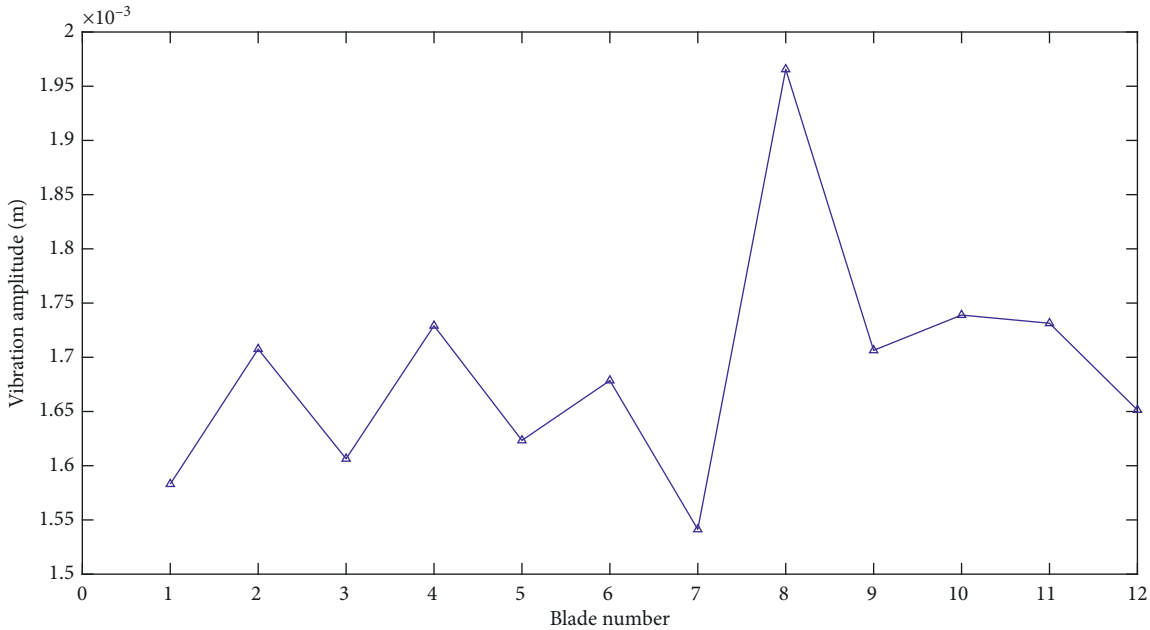

Figure 13: Comparison between vibration amplitudes of blade trunks with no crack occurring.

Since 1x, 2x, and 3x components are relatively obvious, comparison between 1x, 2x, and 3x component peaks is made under different y_c, as shown in Figure 18. It can be seen that, in most cases, peaks of the 1st blade trunk have no significant feature compared with other blade trunks. Therefore, the specific blade trunk where breathing crack occurs cannot be distinguished by comparison between peaks in spectrums.

Next, a comparison between changes in peaks after the occurrence of a breathing crack is made under different y_c, as shown in Figure 19. The change equals value of component peak after crack minus that before crack. It can be seen that after the occurrence of a breathing crack, change in 1x component peak of the 1st blade trunk is the largest, and the differences from others are obvious, under different y_c. Therefore, change in the 1x component peak can be a guidance for determining the specific blade where breathing crack occurs, while in Figures 19(b) and 19(c), changes in 2x and 3x component peaks of the 1st blade trunk do not have an obvious difference comparing others, so they cannot be the features to determine the cracked blade.

To further prove this, a comparison between changes in 1x component peaks of blade trunks is made under different d, as shown in Figure 20. Similar to Figure 19(a), regardless of various d, a change in the 1x component peak of the 1st blade trunk is much larger than others, even when the crack is rather shallow. It is proved again that change in the 1x component peak is suitable as guidance for determining in which blade the breathing crack is located.

5. Conclusions

Cracks are common faults in aeroengine rotated blades, which can result in serious threats to operational safety. Therefore, online vibration monitoring on rotated blades to identify early cracks under various working conditions is significant. As practical form of early cracks, breathing crack can cause nonlinear vibration response on blades. However, as common structures of aeroengine blades, tenon connection and shroud contact can also lead the blades to vibrate nonlinearly, which can seriously interfere with online identification of early cracks. Thus, it is necessary to extract features due to breathing crack in consideration of tenon connection and shroud contact and to provide a theoretical guidance for online identification. An aeroengine rotated blade with tenon and shroud is simplified, and a lumped parameter model of bladed disk is built. Then nonlinear forces on rotated blades are analyzed, and dynamic equations of the lumped parameter model are established. Next, a stiffness model of blade trunk with a breathing crack is launched. Finally, effects on stiffness and vibration response of blade trunks by a breathing crack are studied, based on which effective features are extracted due to breathing crack in time and frequency domains, respectively. Conclusions can be drawn as follows: (i) Tenon connection and shroud contact cause coupling effects between blades, which makes the vibration responses of all blades change once a breathing crack occurs in one of them. Besides, because of the nonlinear characteristics induced by tenon connection and shroud contact, vibration response spectrums of blade trunks consist of 3x and 5x components. (ii) Once breathing crack occurs, vibration amplitude of the cracked blade trunk increases with the distance from blade tip and the depth. However, amplitudes of other trunks fluctuate in random forms because of uncertainties caused by tenon connection and shroud contact; (iii) due to mistuning, localization of vibration response exists. Because of initial differences between vibration amplitudes of blade trunks, whether breathing crack occurs cannot be judged by comparison between amplitudes. But the change in amplitude of the

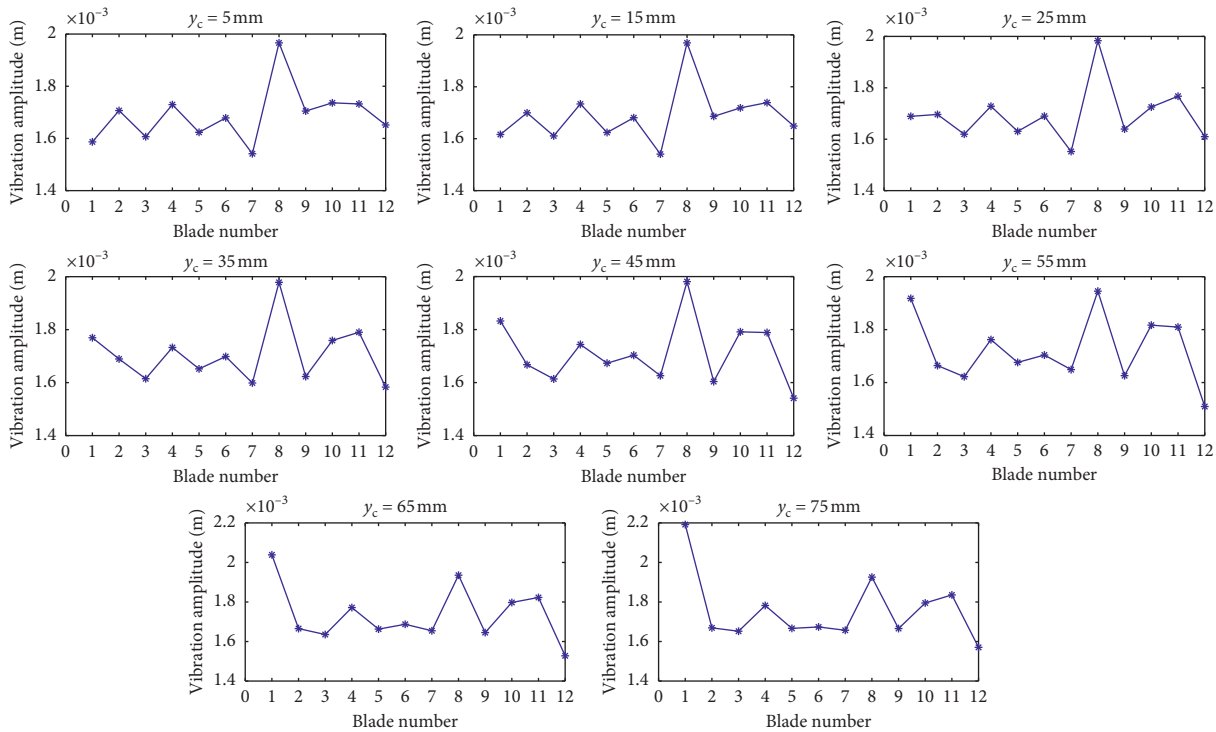

(a)

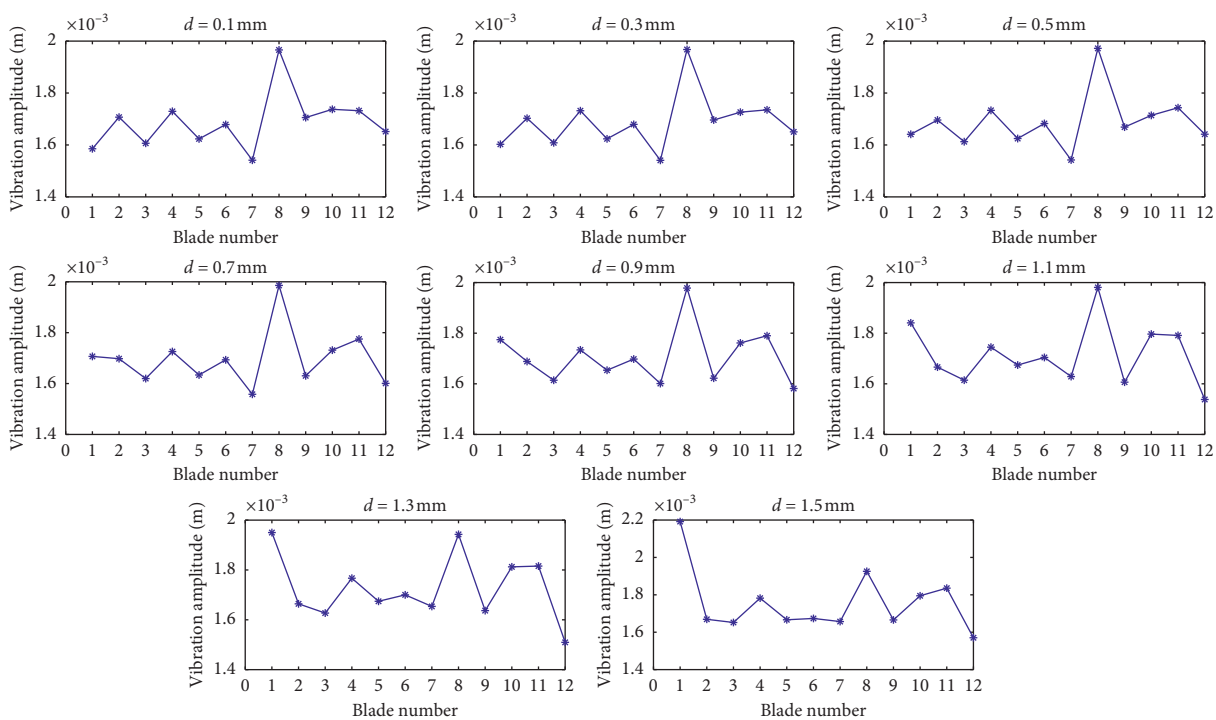

(b)

Figure 14: Comparison between vibration amplitudes of blade trunks when a breathing crack occurs under (a) different distance y_c and (b) different depth d. (a) The depth is set as $d = 1.5$ mm. (b) The distance is set as $y_c = 75$ mm.

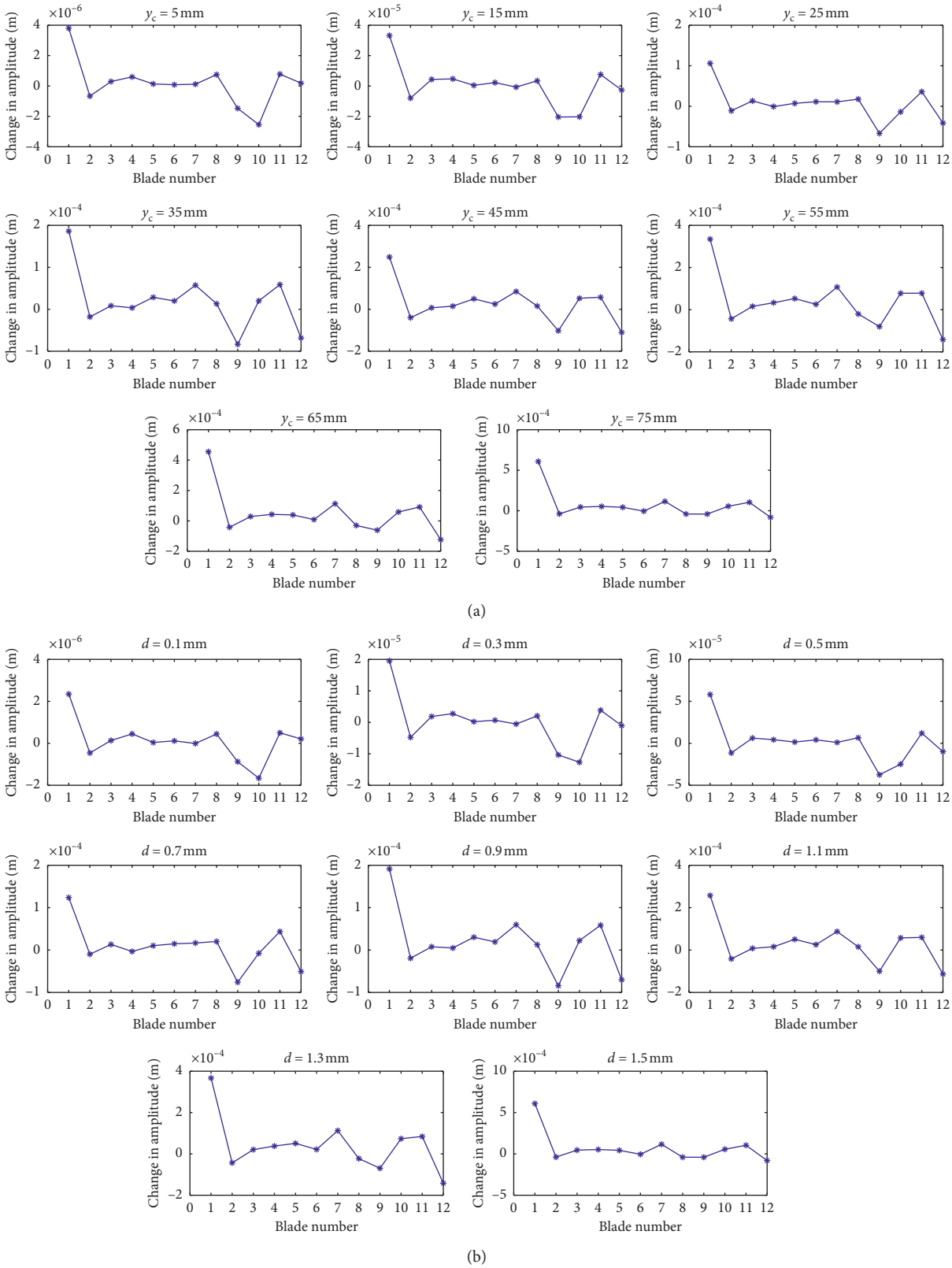

Figure 15: Comparison between the changes in vibration amplitudes of blade trunks after a breathing crack occurs under (a) different distance y_c and (b) different depth d. (a) The depth is set as $d = 1.5$ mm. (b) The distance is set as $y_c = 75$ mm.

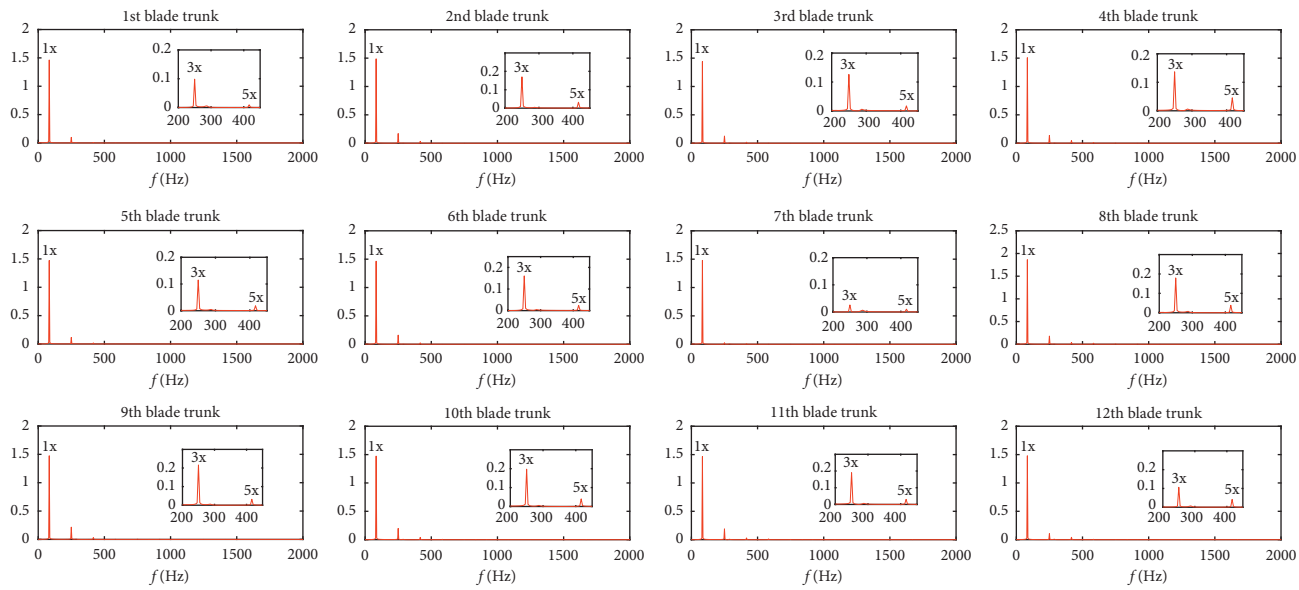

Figure 16: Vibration response spectrum of each blade trunk without crack.

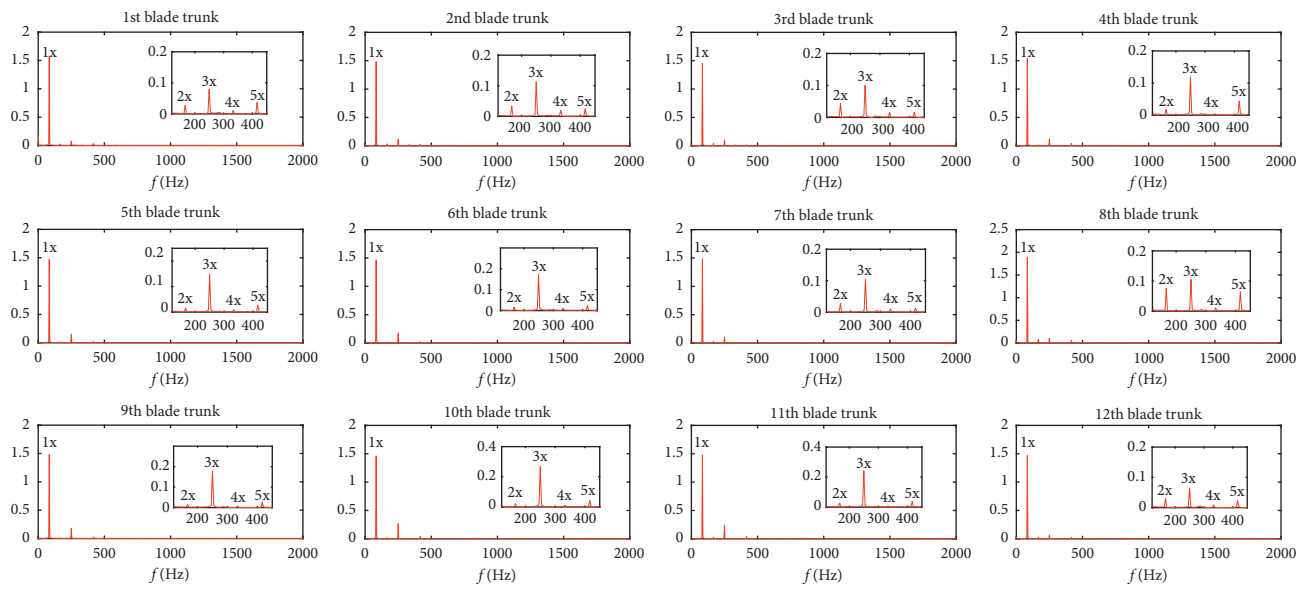

Figure 17: Vibration response spectrum of each blade trunk after a breathing crack occurs. Parameters of the breathing crack are set as follows: $y_c = 45$ mm and $d = 1.5$ mm.

cracked blade trunk is much larger than others, which can be a stable evidence for crack identification. (iv) Breathing crack can cause 2x components in vibration response spectrums because of nonlinear change in the stiffness of the blade trunk. Besides, the specific blade where breathing crack occurs can be distinguished based on the change in the 1x component peak. The findings in this research provide a significant guidance for online identification of breathing crack considering tenon connection and shroud contact.

However, it must be pointed out that this research is still far from practice. Firstly, the subject is a lumped parameter model of simplified bladed disk. But a real bladed disk has a much more complex structure and more factors to affect vibration responses of blades. Secondly, only bending vibrations under airflow excitation are studied in the numerical simulation. Thus, the model proposed should be improved and torsional vibrations of blade trunks should be studied in future. Other forces besides airflow excitation should also be considered. In addition, the features due to breathing crack extracted in this research should be verified in the online identification of early cracks in rotated blades under real working conditions of aeroengine.

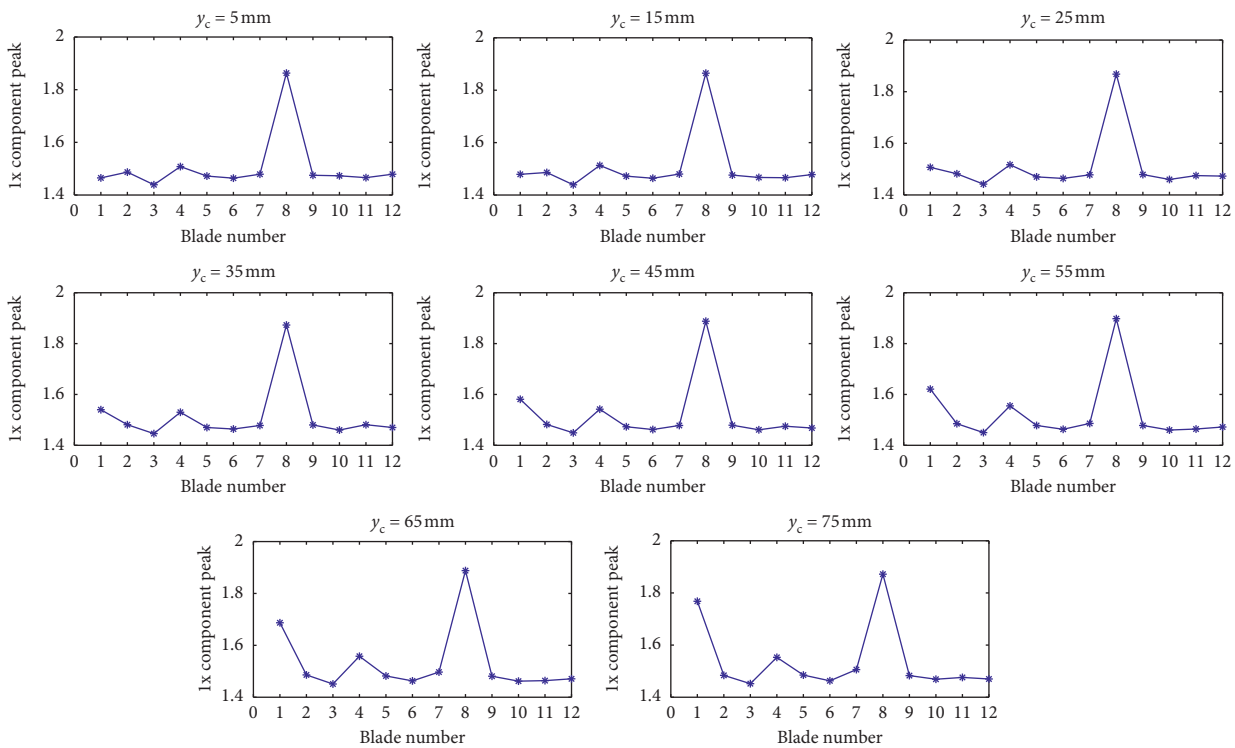

(a)

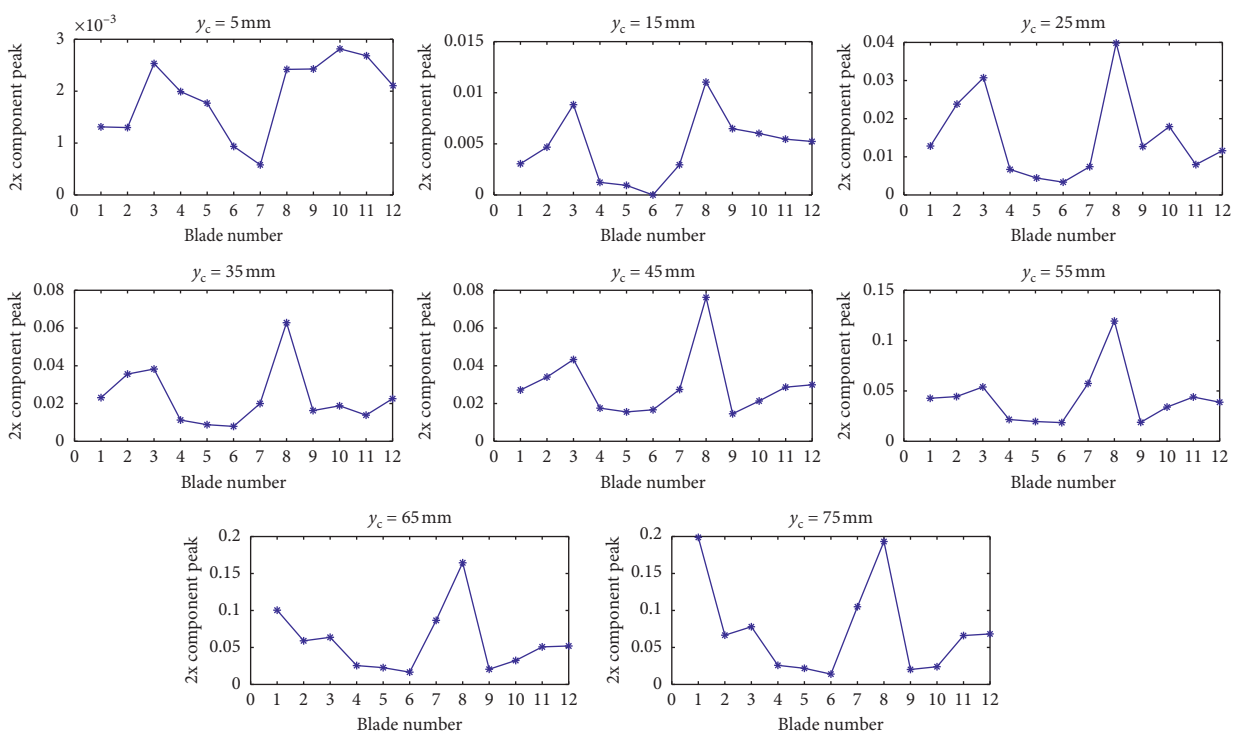

(b)

Figure 18: Continued.

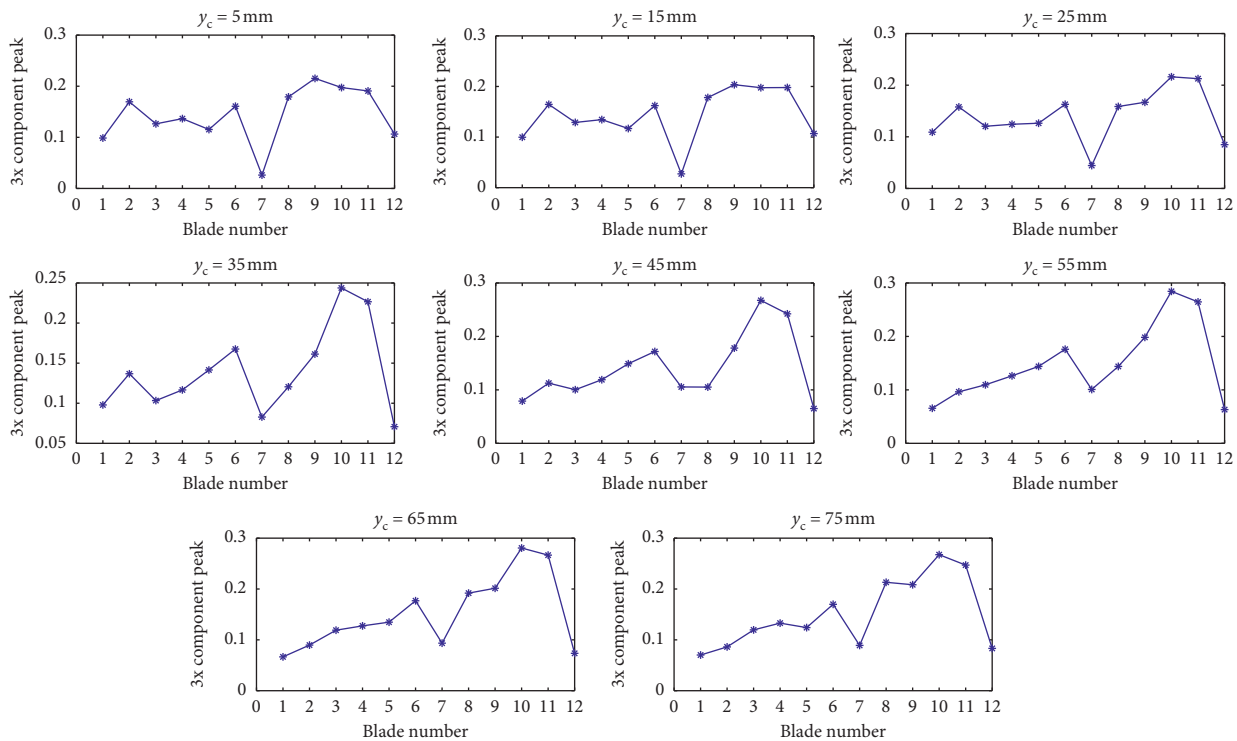

(c)

Figure 18: Comparison between (a) 1x, (b) 2x, and (c) 3x component peaks in vibration response spectrums of blade trunks under different y_c. The depth of the crack is set as d = 1.5 mm.

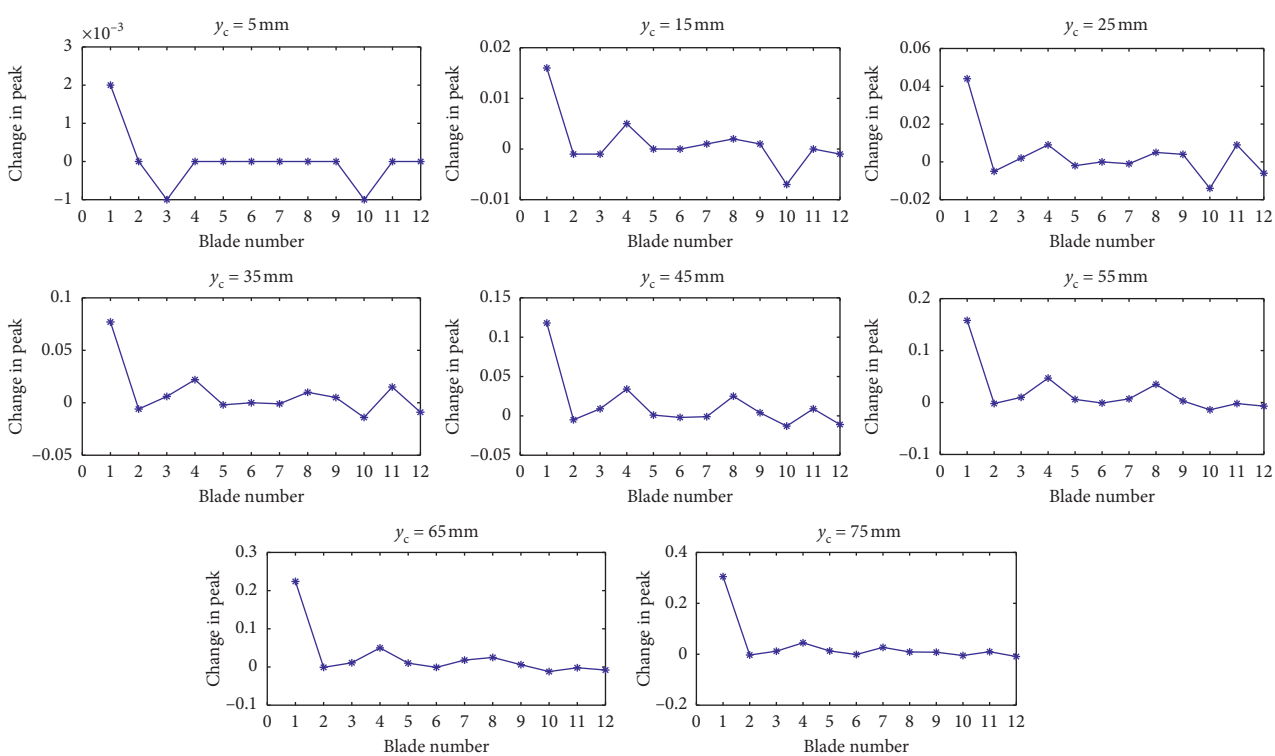

(a)

Figure 19: Continued.

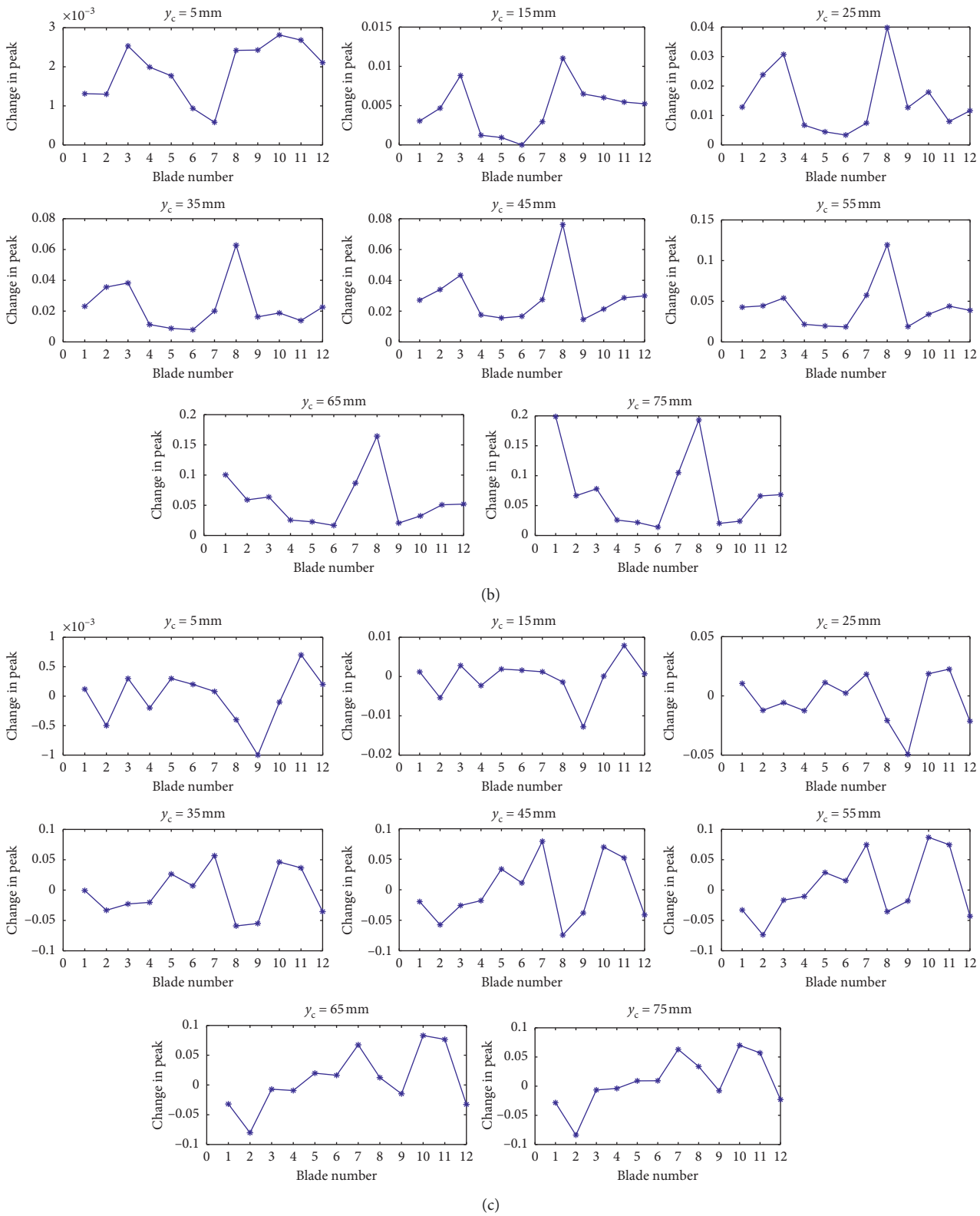

Figure 19: Comparison between changes in (a) 1x, (b) 2x, and (c) 3x component peaks in vibration response spectrums of blade trunks after a breathing crack occurs under different y_c. The depth of the crack is set as $d = 1.5$ mm.

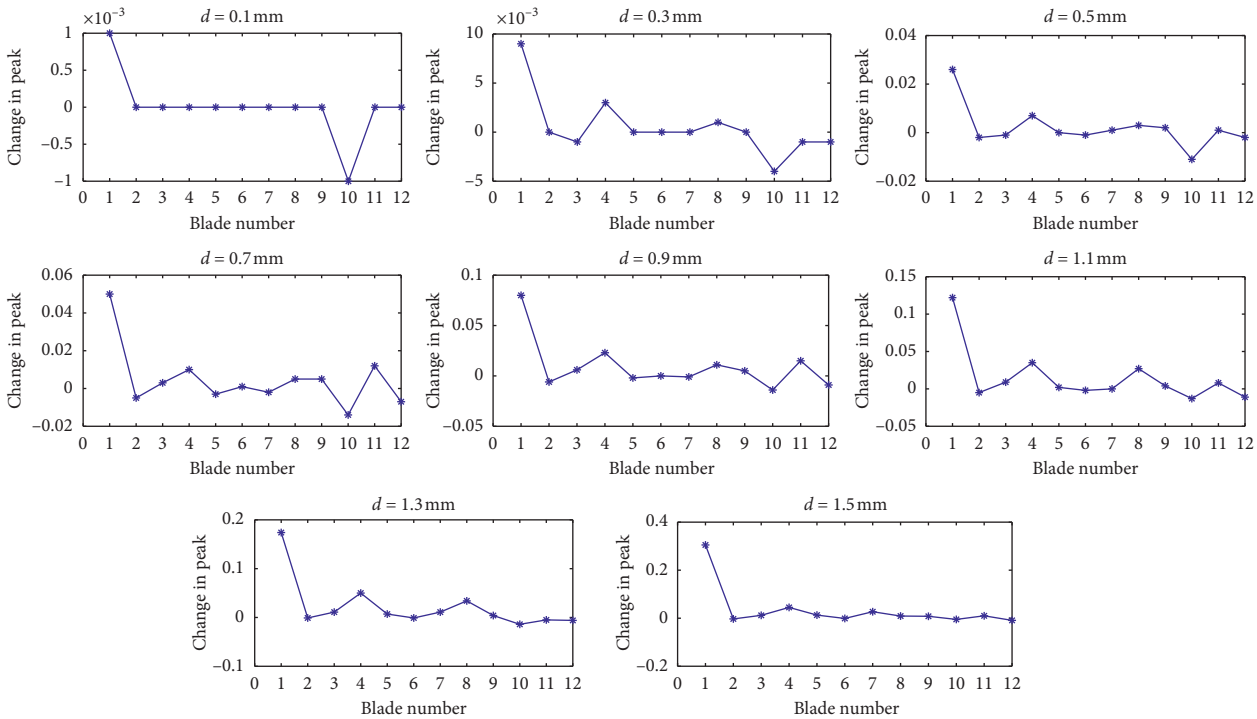

Figure 20: Comparison between changes in 1x component peaks in vibration response spectrums of blade trunks after a breathing crack occurs under different d. The distance of the crack from blade tip is set as $y_c = 75$ mm.

Data Availability

The data used to support the findings of this study are included within the article.

Conflicts of Interest

The authors declare that there are no competing interests regarding the publication of this paper.

Acknowledgments

This work was supported by the National Basis Research Program of China (Grant no. 2015CB057404) and the Natural Science Foundation of Hunan Province, China (Grant no. 2019JJ50721).

References

[1] M. S. Kotambkar, "Exploring vibration based method for crack detection in turbine blade," in *Proceedings of the International Conference on Mechanical & Electrical Technology*, pp. 28–33, Singapore, September 2010.

[2] S. Yang, J. H. Zhang, and J. W. Lin, "Simulation study on crack propagation of aero-engine blade," *Applied Mechanics and Materials*, vol. 105–107, pp. 2153–2156, 2011.

[3] Z. Chen, Y. Yang, Y. Xie, B. Guo, and Z. Hu, "Non-contact crack detection of high-speed blades based on principal component analysis and Euclidian angles using optical-fiber sensors," *Sensors and Actuators A: Physical*, vol. 201, pp. 66–72, 2013.

[4] Z. Chen, J. Liu, C. Zhan, J. He, and W. Wang, "Reconstructed order analysis-based vibration monitoring under variable rotation speed by using multiple blade tip-timing sensors," *Sensors*, vol. 18, no. 10, p. 3235, 2018.

[5] C. Zhan, Z. Chen, Z. Hu, Y. Yang, and H. Hu, "Nonlinear time transformation-based vibration signal reconstruction for blade tip-timing under rotation speed fluctuations," in *Proceedings of the Prognostics and System Health Management Conference*, pp. 237–241, Harbin, China, July 2017.

[6] L. Zhang, H. Yuan, Q. Han, S. Yang, L. Song, and Y. Li, "Vibration analysis of mistuned bladed disk system based on microslip friction model," *Journal of Vibration Engineering*, vol. 25, no. 3, pp. 289–293, 2012.

[7] D. Zhang, J. Fu, Q. Zhang, and J. Hong, "An effective numerical method for calculating nonlinear dynamics of structures with dry friction: application to predict the vibration response of blades with underplatform dampers," *Nonlinear Dynamics*, vol. 88, no. 1, pp. 223–237, 2017.

[8] E. P. Petrov, "Analysis of flutter-induced limit cycle oscillations in gas-turbine structures with friction, gap, and other nonlinear contact interfaces," *Journal of Turbomachinery*, vol. 134, no. 6, Article ID 061018, 13 pages, 2012.

[9] B.-D. Yang and C.-H. Menq, "Modeling of friction contact and its application to the design of shroud contact," *Journal of Engineering for Gas Turbines and Power*, vol. 119, no. 4, pp. 958–963, 1997.

[10] M.-C. Wu and S.-C. Huang, "On the vibration of a cracked rotating blade," *Shock & Vibration*, vol. 5, no. 5-6, pp. 317–323, 1998.

[11] C. He, H. Li, and X. Zhao, "Weak characteristic determination for blade crack of centrifugal compressors based on underdetermined blind source separation," *Measurement*, vol. 128, pp. 545–557, 2018.

[12] P. Gudmundson, "The dynamic behaviour of slender structures with cross-sectional cracks," *Journal of the Mechanics and Physics of Solids*, vol. 31, no. 4, pp. 329–345, 1983.

[13] F. Ismail, A. Ibrahim, and H. R. Martin, "Identification of fatigue cracks from vibration testing," *Journal of Sound and Vibration*, vol. 140, no. 2, pp. 305–317, 1990.

[14] S. M. Cheng, A. S. J. Swamidas, X. J. Wu, and W. Wallace, "Vibrational response of a beam with a breathing crack," *Journal of Sound and Vibration*, vol. 225, no. 1, pp. 201–208, 1999.

[15] C. Liu, D. Jiang, and F. Chu, "Influence of alternating loads on nonlinear vibration characteristics of cracked blade in rotor system," *Journal of Sound and Vibration*, vol. 353, pp. 205–219, 2015.

[16] H. Xu, Z. Chen, Y. Xiong, Y. Yang, and L. Tao, "Nonlinear dynamic behaviors of rotated blades with small breathing cracks based on vibration power flow analysis," *Shock and Vibration*, vol. 2016, Article ID 4197203, 11 pages, 2016.

[17] D. Laxalde and F. Thouverez, "Complex non-linear modal analysis for mechanical systems: application to turbomachinery bladings with friction interfaces," *Journal of Sound and Vibration*, vol. 322, no. 4-5, pp. 1009–1025, 2009.

[18] C. Li, Z. Shen, B. Zhong, and B. Wen, "Study on the nonlinear characteristics of a rotating flexible blade with dovetail interface feature," *Shock and Vibration*, vol. 2018, Article ID 4923898, 13 pages, 2018.

[19] H. Zeng, S. Cao, and Y. Su, "Vibration localization of a mistuned bladed disk system with friction and gap," *Journal of Vibration and Shock*, vol. 35, no. 2, pp. 82–90, 2016.

[20] B. D. Yang, M. L. Chu, and C. H. Menq, "Stick–slip–separation analysis and non-linear stiffness and damping characterization of friction contacts having variable normal load," *Journal of Sound and Vibration*, vol. 210, no. 4, pp. 461–481, 1998.

[21] B. H. Ji, G. H. Zhang, L. T. Wang, Q. Yuan, Q. J. Meng, and D. Y. Liu, "Experimental investigation of the dynamic characteristics of the damped blade," *Journal of Sound and Vibration*, vol. 213, no. 2, pp. 223–234, 1998.

[22] J. Voldřich, P. Polach, J. Lazar, and T. Míšek, "Use of cyclic symmetry properties in vibration analysis of bladed disks with friction contacts between blades," *Procedia Engineering*, vol. 96, pp. 500–509, 2014.

[23] J. Wu, L. Tan, D. Zhang, and Y. Xie, "Experimental study on vibration characteristics of dry friction damping of turbine blade with integral shroud," *Proceedings of the Chinese Society of Electrical Engineering*, vol. 30, no. Sl, pp. 110–116, 2010.

[24] G. C. Zhou, Z. X. Wen, Z. F. Yue, and Y. F. Gao, "The influence of friction coefficient on tenon/groove contact performance in nickel-based turbine blade-disc," *Advanced Materials Research*, vol. 940, pp. 74–80, 2014.

[25] S. Zhang, X. Shen, S. Dong, Z. Ye, and W. Hu, "A method to analyze the contact stress of dovetail attachments in aero-engine," *Journal of Engineering for Gas Turbines and Power*, vol. 141, no. 2, Article ID 022505, 10 pages, 2018.

[26] B. Santhosh, S. Narayanan, and C. Padmanabhan, "Nonlinear dynamics of shrouded turbine blade system with impact and friction," *Applied Mechanics & Materials*, vol. 706, pp. 81–92, 2014.

[27] S.-T. Wei and C. Pierre, "Effects of dry friction damping on the occurrence of localized forced vibrations in nearly cyclic structures," *Journal of Sound and Vibration*, vol. 129, no. 3, pp. 397–416, 1989.

[28] C.-H. Menq, J. H. Griffin, and J. Bielak, "The influence of a variable normal load on the forced vibration of a frictionally damped structure," *Journal of Engineering for Gas Turbines and Power*, vol. 108, no. 2, pp. 300–305, 1986.

[29] H. Xu, Z. Chen, Y. Yang, L. Tao, and X. Chen, "Effects of crack on vibration characteristics of mistuned rotated blades," *Shock and Vibration*, vol. 2017, Article ID 1785759, 18 pages, 2017.

[30] S.-T. Wei and C. Pierre, "Localization phenomena in mistuned assemblies with cyclic symmetry Part II: forced vibrations," *Journal of Vibration Acoustics Stress and Reliability in Design*, vol. 110, no. 4, pp. 439–449, 1988.